The Arthrotropism of Macromolecules in Adjuvant-Induced Arthritis Rat Model: A Preliminary Study

Dong Wang,[1,5] Scott C. Miller,[3] Monika Sima,[1] Dennis Parker,[4] Henry Buswell,[4] K. Craig Goodrich,[4] Pavla Kopečková,[1] and Jindřich Kopeček[1,2,5]

Received April 21, 2004; accepted June 28, 2004

Purpose. To study the accumulation of macromolecules into the arthritic joints and the possible applications of such phenomenon.
Methods. The accumulation of plasma albumin in the joints of adjuvant-induced arthritis (AIA) rat model was first visualized with Evans blue injection. A *N*-(2-hydroxypropyl)methacrylamide (HPMA) copolymer contrast agent was then synthesized and injected into the AIA rats to allow qualitative examination of biodistribution and pharmacokinetics of the injected macromolecule with magnetic resonance imaging (MRI). Vital organs and the diseased joints were isolated and examined histologically to correlate with the MRI findings.
Results. Deep blue color developed around the arthritic joints of the AIA rat a few hours after the injection of Evans blue. MR imaging of the AIA rats injected with polymer contrast agent demonstrated a gradual but very strong accumulation of the injected polymer in the arthritic joints, which lasted for 1~2 days. Observed differences in the concentration of the injected polymer in the joints correlated with disease severity as assessed histologically.
Conclusions. Profound arthrotropism of macromolecules in the AIA rat model was demonstrated with various imaging tools. These observations should help in the conceptual and practical design of novel macromolecular delivery systems for the imaging and treatment of rheumatoid arthritis.

KEY WORDS: arthrotropism; drug delivery; macromolecular therapy; macromolecule; magnetic resonance imaging (MRI); rheumatoid arthritis.

[1] Department of Pharmaceutics & Pharmaceutical Chemistry, University of Utah, Salt Lake City, Utah 84112, USA.
[2] Department of Bioengineering, University of Utah, Salt Lake City, Utah 84112, USA.
[3] Division of Radiobiology, University of Utah, Salt Lake City, Utah 84112, USA.
[4] Department of Radiology, University of Utah, Salt Lake City, Utah 84112, USA.
[5] To whom correspondence should be addressed. (e-mail: dong.wang@m.cc.utah.edu; Jindrich.Kopecek@m.cc.utah.edu)

INTRODUCTION

Rheumatoid arthritis (RA) is the most common inflammatory arthritis, affecting about 1% of the general population worldwide. In the United States, about 4.5% of people over the age of 55 have been affected (1,2).

As a symmetric disease, RA usually involves the same joints on both sides of the body. Angiogenesis and microvascular lesions are common features of RA inflammation, which leads to abnormal serum protein infiltration into the synovia (3–5). Clearance of synovial fluid and its constituents was reported to be increased in inflamed joints as a result of increased lymphatic drainage (4), though damaged or depleted lymphatics have been observed in the synovium of RA patients as well (6,7).

Although the exact cause of rheumatoid arthritis is unknown, many medications have been developed to relieve its symptoms and slow or halt its progression. Most commonly used medications rest on two principal approaches: symptomatic treatment with non-steroidal anti-inflammmatory drugs (NSAIDs) and disease-modifying antirheumatic drugs (DMARDs) (3).

Considerable effort has been made to identify and develop new therapeutic strategies for the treatment of RA. Novel RA medications, such as cycloxygenase-2 (COX-2) specific inhibitors (a NSAID) (8), tumor necrosis factor (TNF) blockers and interleukin-1 receptor antagonists (IL-1Ra) (DMARDs) have been used for clinical applications (3). However, little attention has been paid to the pharmaceutical improvement of the available RA drugs to make them more efficient. In fact, many of the available treatments have various side effects, which limit their clinical application. Well-known side effects of NSAIDs include indigestion, stomach bleeding, liver and kidney damage, ringing in ears (tinnitus), fluid retention and high blood pressure (9). Well-known side effects of glucocorticoids include bruising, thinning of bones, cataracts, weight gain, redistribution of fat, diabetes and high blood pressure (10). Some DMARDs are immunosuppressants and their application can potentially lead to serious side effects, such as increased susceptibility to infection (3). Even with the newly developed COX-2 specific inhibitors, there are concerns about their side effects on kidney and bone (9).

With oral or systemic administration of these drugs, some side effects arise from their profound physiologic activity in many tissues other than the inflamed joints. The clinical dosing range of these therapeutics is kept relatively low to avoid the side effects, which would also reduce the efficacy of

ABBREVIATIONS: AIA, adjuvant induced arthritis; AIBN, 2,2'-azobisisobutyronitrile; APMA, *N*-(3-aminopropyl)methacrylamide hydrochloride; COX-2, cycloxygenase-2; DMARDs, disease-modifying antirheumatic drugs; DIPEA, diisopropylethyl amine; DOTA, 1,4,7,10-tetraazacyclododecane-1,4,7,10-tetra(acetic acid); DOTA-NHS ester, 1,4,7,10-tetraazacyclododecane-1,4,7-tris(acetic acid)-10-acetic acid mono (*N*-hydroxysuccinimidyl ester); EB, Evans blue; EPR, enhanced permeability and retention; FITC, fluorescein isothiocyanate; FPLC, fast protein liquid chromatography; HPMA, *N*-(2-hydroxypropyl)methacrylamide; ICP-OES, inductively coupled plasma optical emission spectroscopy; IL-1Ra, interleukin-1 receptor antagonist; LA, *N*,*N*-dioctadecyl-*N*',*N*'-bis(2-hydroxyethyl) propanediamine; MA-FITC, *N*-methacryloylaminopropyl fluorescein thiourea; M_n, number average molecular weight; MPA, 3-mercaptopropionic acid; MRI, magnetic resonance imaging; M_w, weight average molecular weight; NSAIDs, symptomatic treatment with non-steroidal anti-inflammmatory drugs; OA, osteoarthritis; OMNISCAN, or gadodiamide is the injectable formulation of the gadolinium complex of diethylenetriamine pentaacetic acid bismethylamide; PHPMA, poly[*N*-(2-hydroxypropyl)methacrylamide]; Poly(HPMA-*co*-APMA-*co*-MA-FITC), copolymer of HPMA, APMA and MA-FITC; P-DOTA, conjugation product of poly(HPMA-*co*-APMA-*co*-MA-FITC) and DOTA-NHS ester; P-DOTA-Gd^{3+}, purified complex of P-DOTA and Gd^{3+}; RA, rheumatoid arthritis; R.T., room temperature; SEC, size exclusion chromatography; TNF, tumor necrosis factor.

the drugs on the RA joints. Therapeutic delivery systems, which could specifically deliver antiarthritis drugs to the inflamed joints of RA patients may avoid many of the side effects expressed in other tissues while achieving much greater clinical therapeutic efficacy.

The application of water-soluble polymers as drug carriers for effective delivery of the drug to the desired sites (macromolecular therapy) has been extensively studied for the past two decades in the treatment of solid tumors (11). Because of the "leaky" vasculature and poorly developed lymphatic system, extravasated macromolecules preferentially accumulate in solid tumors. This phenomenon is termed tumor-selective "enhanced permeability and retention" (EPR) effect and has been used successfully to target anti-cancer drugs to solid tumors (12).

In spite of some pathophysiological similarity between solid tumor and RA joints, such as extensive angiogenesis and leaky vasculature, only a few attempts have been made to apply the concept of macromolecular therapy in the treatment of RA. Studies using micro-particulate carriers, such as liposomes for the delivery of anti-arthritic agents to the RA joint have shown some promising results in an animal model of arthritis (13). However, because of the existence of lymphatic drainage, different retention kinetics of macromolecules may be expected in RA joints compared to solid tumors.

Magnetic resonance imaging (MRI) is a noninvasive method of mapping the internal structure of the body. MRI employs radiofrequency (RF) radiation in the presence of carefully controlled magnetic fields in order to produce high quality cross-sectional images of the body in any plane. It portrays the distribution of hydrogen nuclei and parameters relating to their motion in water and lipids. Introduction of paramagnetic contrast agents would shorten T_1 (the longitudinal relaxation time) of the hydrogen nuclei in tissues, which in turn will increase the MR signal intensity thereof (14).

In the current study, we synthesized a macromolecular MRI contrast agent based on *N*-(2-hydroxypropyl)methacrylamide (HPMA) copolymer. After systemic administration of the contrast agent in an adjuvant-induced arthritis (AIA) rat model, contrast-enhanced MR images were taken to follow the distribution of the polymer at different time points. Correlating the MR results with additional visual and histopathological results from the AIA rats, we clearly demonstrate the preferential deposition and retention of macromolecules to the inflamed joints. These observations support the concept of using macromolecular therapy for the treatment of rheumatoid arthritis. This same concept may also be applied to improved imaging and diagnosis of rheumatoid arthritis. The suitable designs of the polymeric delivery systems and the possible selection of antiarthritic drugs are discussed as well.

MATERIALS AND METHODS

Materials

N-(2-hydroxypropyl)methacrylamide (HPMA) (15), *N*-methacryloylaminopropyl fluorescein thiourea (MA-FITC) (16), and *N*,*N*-dioctadecyl-*N*',*N*'-bis(2-hydroxyethyl) propanediamine (17) were prepared as described previously. 2,2'-Azobisisobutyronitrile (AIBN) and 3-mercaptopropionic acid (MPA) were obtained from Aldrich (Milwaukee, WI, USA). Sephadex G-25 and LH-20 beads were obtained from Amersham Biosciences Corporation (Piscataway, NJ, USA). *N*-(3-Aminopropyl)methacrylamide hydrochloride (APMA) was obtained from Polysciences, Inc. (Warrington, PA, USA). 1,4,7,10-Tetraazacyclododecane-1,4,7-tris(acetic acid)-10-acetic acid mono (*N*-hydroxysuccinimidyl ester) (DOTA-NHS ester) was obtained from Macrocyclics (Dallas, TX, USA). *N*-(3-Aminopropyl)diethanol amine was obtained from TCI America (Portland, OR, USA). An injectable formulation of the gadolinium complex of diethylenetriamine pentaacetic acid bismethylamide (OMNISCAN) was obtained from Amersham Health Inc. (Princeton, NJ, USA). *Mycobacterium tuberculosis* H37Ra (heat killed, desiccated) was obtained from VWR International (West Chester, PA, USA). Paraffin oil (low viscosity, Bayol F) was obtained from Crescent Chemical Company, Inc. (Islandia, NY, USA). If not specified, all other reagents and solvents were purchased from Aldrich (Milwaukee, WI, USA).

Characterization of the Synthetic Products

The weight average molecular weight (M_w) and number average molecular weight (M_n) of polymers were determined by size exclusion chromatography (SEC) using the ÄKTA FPLC system (Amersham Pharmacia Biotech) equipped with UV and RI detectors. SEC measurements were carried out on Superose 12 columns (HR 10/30) with PBS (pH = 7.3) as the eluent. The average molecular weights of the polymers were calculated using calibrations with poly[*N*-(2-hydroxypropyl)methacrylamide] (PHPMA).

UV spectra of FITC containing polymer were obtained on a Cary 400 Bio UV-Visible spectrometer (Varian).

^{1}H NMR spectra of all synthesized compounds were recorded on a Varian Unity 500 MHz NMR spectrometer. The solvent peak was used for reference (d_6-DMSO, 2.49 ppm).

Mass spectra of all synthesized compounds were obtained using a Finnigan LCQ DECA Mass Spectrometer interfaced to an ESI source.

MRI Procedure

MR images of the animals were acquired on a 1.5 T Signa LX imaging system (General Electric Medical Systems, Milwaukee, WI, USA), using a 2-element phased-array receive only coil, where each coil was 9 × 11 cm and the combined pair was 17 × 11 cm. The coils were overlapped so that the mutual inductance between coils was negligible. Images were acquired using a 3D single slab IR prepared FSPGR sequence in the coronal plane. The common imaging parameters were TR = 13.4 ms, TE = 2.2 ms, TI = 300 ms, 25° flip angle, 512 × 256 in-plane acquisition matrix, 20 × 10 cm^2 field-of-view (FOV), 64 slices per slab, 1.0 mm thick slices with 2 × interpolation to 0.5 mm.

Synthesis of Poly(HPMA-*co*-APMA-*co*-MA-FITC)

HPMA (1 g, 7 mmol), APMA (0.14 g, 0.78 mmol), MA-FITC (0.043 g, 7.8 μmol), AIBN (0.057 g, 0.35 mmol), and MPA (0.001 ml, 1 μmol) were dissolved in methanol (10 ml), placed in an ampoule, and purged with N_2 for 5 min. The ampoule was flame-sealed and maintained at 50°C for 24 h. The polymer was isolated by precipitation of the resulting

solution into acetone and was reprecipitated twice. After the polymer was dried in desiccator (over NaOH), the final yield was determined as 0.9 g. The content of free amino groups in the copolymer was determined as 7.7×10^{-4} mol/g using the ninhydrin assay (18).

Synthesis of P-DOTA [Conjugate of Poly(HPMA-*co*-APMA-*co*-MA-FITC) with DOTA-NHS Ester]

Poly(HPMA-*co*-APMA-*co*-MA-FITC) (170 mg, $[NH_2] = 1.33 \times 10^{-4}$ mol), DOTA-NHS ester (100 mg, 2×10^{-4} mol), and diisopropylethyl amine (DIPEA, 160 μl, 9.33×10^{-4} mol, distilled from ninhydrin) were mixed in DMF (1.5 ml, distilled from P_2O_5) and stirred overnight. The conjugate was precipitated into ether and dried under vacuum. The product was further purified on LH-20 column, dialyzed (molecular weight cutoff size 6-8 kDa) and lyophilized to obtain 190 mg of final product. The amount of residual free NH_2 groups were determined with ninhydrin assay and the content of DOTA in the product was calculated as 7.5×10^{-4} mol/g.

Synthesis and Purification of Macromolecular MRI Contrast Agent P-DOTA-Gd^{3+}

P-DOTA (100 mg, [DOTA] = 6.9×10^{-5} mol) and $GdCl_3 \cdot 6H_2O$ (38 mg, 1.04×10^{-4} mol) were dissolved in 2 ml deionized H_2O. The pH of the solution was maintained at 5.0–5.5 overnight by gradual addition of 1 N NaOH solution. EDTA disodium salt (38 mg, 1.04×10^{-4} mol) was then added into the solution to chelate the excess Gd^{3+}. After stirring for 30 min, the milky solution was purified with Sephadex G-25 column to remove the EDTA-chelated Gd^{3+} and other unreacted low molecular weight compounds from the polymer conjugate. The conjugate was lyophilized to yield 115 mg P-DOTA-Gd^{3+}. The gadolinium content was determined by Inductively Coupled Plasma Optical Emission Spectroscopy (ICP-OES) as 0.52 mmol/g. The M_w of the polymeric MRI contrast agent determined by SEC was 55 kDa with a polydispersity of 1.4. This is close to the glomerular filtration threshold of 45 kDa for HPMA copolymer (19) to ensure urinary clearance from the body. The T_1 relaxivity of the conjugate was determined as 10.4 $mm^{-1}s^{-1}$ per complexed Gd^{3+} using a B1 homogeneity corrected Look-Locker technique on the 1.5T GE NV/CVi scanner with the LX 8.4 operating system at room temperature (20). The chemical structure of the macromolecular MRI contrast agent is shown in Fig. 1.

Adjuvant-Induced Arthritis Rat Model

Male Lewis rats (175–200 g) were obtained from Charles River Laboratories (Portage, MI, USA) and allowed to acclimate for at least 1 week. To induce arthritis, *Mycobacterium tuberculosis* H37Ra (1 mg) and *N*,*N*-dioctadecyl-*N*',*N*'-bis(2-hydroxyethyl) propanediamine (LA, 5 mg) were mixed in paraffin oil (100 μl), sonicated and s.c. injected into the base of the rat's tail (21). The rats were then randomized into 3 rats/group. The progression of the joint inflammation was followed by measuring the diameter of the ankle joint with a digital caliper. Special care was given to the rats as the inflammation developed to ensure availability and access to water and food. The MRI contrast agents used for the study

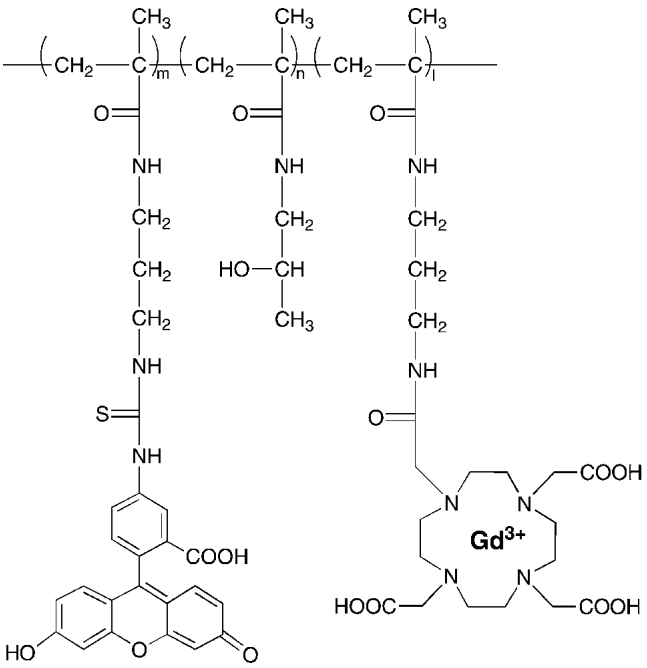

Fig. 1. Chemical structure of the macromolecular MRI contrast agent (P-DOTA-Gd^{3+}) used in this study.

were injected directly into the jugular vein while the animal was anesthetized with ketamine and xylazine. All animal experiments were performed according to a University of Utah IACUC approved protocol and adhered to the "Principles of Laboratory Animal Care" (NIH Publication No. 85-23, revised in 1985).

Visualization of Plasma Albumin Accumulation in RA Joints

Evans blue dye (EB, 10 mg/kg in saline) was injected into healthy and AIA rats via the tail vein. The extravasation and accumulation of dye in the areas of joint inflammation could be visually observed by the appearance of the blue pigment. Photographs of the ankle and paws were taken before and 8 h after injection.

Histology

At necropsy, the major organs and limbs were removed and fixed with 10% phosphate buffered formalin for 24 h. The organs were then dehydrated and embedded in paraffin for routine histopathological analyses. The limbs were gradually dehydrated in ascending concentrations of ethanol and embedded in poly(methyl methacrylate). Sections of the entire joint, including the bone, were cut with a low speed saw using diamond-wafering blades. The sections were mounted on plastic slides, ground to about 50 μm in thickness and surface stained using a Giemsa stain modified for plastic sections (22). The joints (knee, ankle, tarsals and metatarsals) from the same animals that were imaged by MRI were assessed for the presence of inflammation and tissue damage.

RESULTS

Visual and Histologic Examination of AIA Rats

The development of adjuvant-induced arthritis in the rat is well described in the literature (21), and briefly summarized

here. After injection of the adjuvant, changes begin to become evident about 9 days later. This includes some inflammation around the eyes and enlarged and tender external genitalia. Inflammation and swelling of the front and hind limb ankle joints becomes evident at about 12 days after injection of the adjuvant.

At necropsy on 15 days postinjection of the adjuvant, inflammation of the peritoneum (peritonitis) can be observed. Occasionally, inflammation of gastrointestinal (GI) tract and fluid retention in the peritoneal cavity are also detectable. Grossly, most of the vital organs appear to be normal except that the spleen is usually enlarged with visual evidence of inflammation.

However, under histopathological examination, all organs examined showed signs of chronic inflammation. The testicular tissue demonstrated inflammation in the membranes around the testis, with small granulomata in the epididymis being detected. The pericardial tissue demonstrated chronic inflammation, which easily could allow for build up of fluid in the pericardial tissue. The renal tissue included multifocal areas of granulomata formation in the cortical tissue with some inflammation over the capsule, particularly along potential serosal surface changes. The splenic tissue demonstrates multifocal areas of necrosis surrounded by neutrophils and epithelioid cells. Plasma cells and lymphocytes are responding around this process, which indicate a rather severe inflammatory response throughout the splenic tissue.

Some of the histologic features of the joints from the hind limbs of the AIA rats are presented in Fig. 2. At lower magnification, the swelling and inflammation of the ankle joint region and paws of the AIA rats were readily apparent (Fig. 2A). Extensive cartilage, joint and bone destruction were also associated with the local inflammation (Figs. 2B to 2D). The larger vessels in the inflammatory regions had a thickened, but vacuolated endothelium (Fig. 2E). By contrast, the knee joints from the AIA rats were typically less affected by the inflammatory process, except for small inflammatory foci (Fig. 2F).

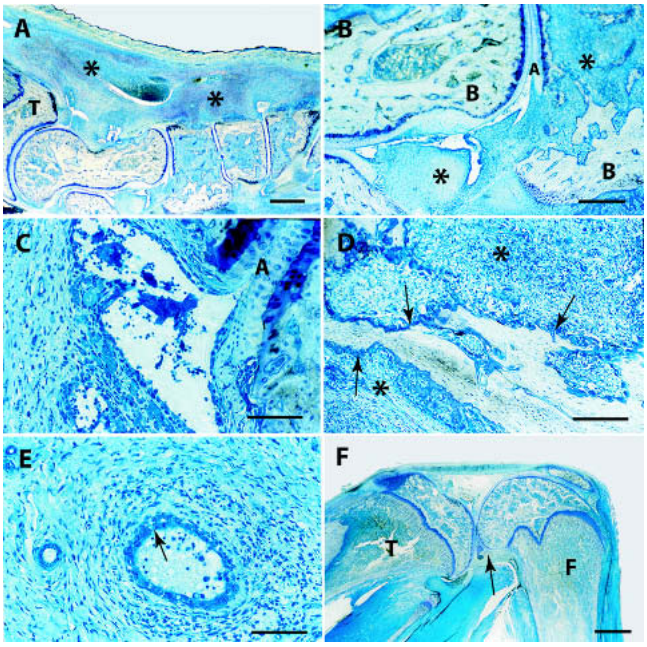

Fig. 2. Histology of the ankle and knee joints from the same AIA rats imaged by MRI. All samples were stained using a Giemsa stain modified for plastic embedded undecalcified bone sections. (A) Low-power micrograph of the ankle and foot bones. Extensive swelling and inflammation are evident in the soft tissues (*) surrounding the foot bones. T = tibia. Bar = 1 mm. (B) Tarsal joint illustrating synovial inflammation (synovitis) with extensive inflammatory cell infiltration (*) and cartilage and bone destruction. B = bone, A = articular cartilages. Bar = 0.5 mm. (C) Higher magnification of the inflammation in the synovial tissues. A = articular cartilage. Bar = 100 μm. (D) Extensive bone destruction with inflammatory infiltration (*) in a tarsal (ankle) bone. Bone surfaces are lining with large active osteoclasts adjacent to eroded bone surfaces (arrows). Bar = 200 μm. (E) Several blood vessels in an inflamed region of the ankle joint illustrating the inflammatory reaction around the vessels. The endothelial lining is thickened and vacuolated (arrows). Bar = 100 μm. (F) A low-power micrograph of the knee joint from this same animal. The joint is quite normal in appearance except for a small pocket of inflammation on the posterior aspect of the joint (arrow). The MR contrast signal of the same area was enhanced when observed by MRI. T = tibia; F = femur. Bar = 2 mm.

Visual Examination of the AIA Rats After Evans Blue Injection

For this study, EB was injected into the rats 15 days after injection of the adjuvant. By this time, there was a robust inflammatory reaction evident in the ankle joints. After injection of EB, there was a gradual accumulation of blue color in the inflamed hind paw and front paws of the AIA rats with high density of the color located around the tarsus and carpus. Some deep blue spots were also observed on some digits of the paw. Photographs taken before and after injection of the EB dye (data not shown) confirm that the areas with dye accumulation correspond to those with marked inflammation. In the healthy control rats given EB, the dye was not localized to joint areas as observed in the AIA rats.

MR Imaging

Imaging AIA Rats with P-DOTA-Gd^{3+} as a Contrast Agent

Immediately prior to the injection of the P-DOTA-Gd^{3+} contrast agent, a baseline MRI scan was done. The animals were then injected with the contrast agent and MRI scans were performed at different time intervals. The acquired images were post-processed using the maximum intensity projection (MIP) algorithm. The resulting MIP images of the animals are depicted chronologically in Fig. 3.

As shown in the baseline image (Fig. 3A) before contrast injection, the intestine and stomach of the animal are clearly visible likely due to fluid retention. Several irregular spots are also observed in the lower abdomen, which can be attributed to i.p. injection site(s) of anesthetic agents. An area in the scrotum, adjacent to the testes in the anatomic region of the epididymus and associated tissue also shows a diffuse MR signal, perhaps due to its fatty content or accumulation of fluid. The bright spot at the right sciatic region may represent the fluid retention in an inconsistent lymph node called *lc. ischiadicum*, which is also evident is some of the subsequent images from this animal. No significant MR signal was observed at the hind limbs. The ankle joints were, however, clearly enlarged in the latent image when compared with similar images of the controls.

At 5 min after the injection of the macromolecular con-

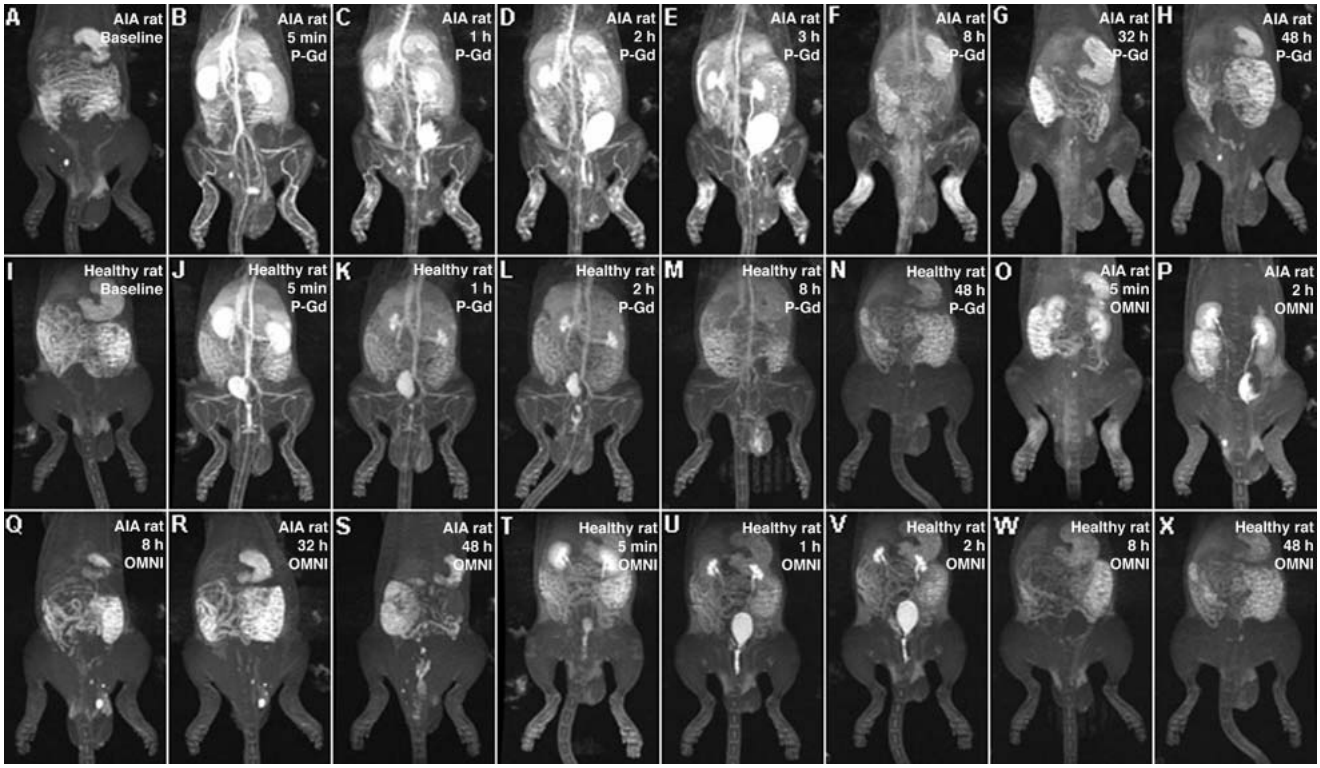

Fig. 3. The MR images of the animals taken at different time points. The acquired images were post-processed using the maximum intensity projection (MIP) algorithm. P-DOTA-Gd^{3+} is abbreviated as P-Gd; OMNISCAN is abbreviated as OMNI in the individual MR image explanation. (A–H) AIA rat images at baseline (A) and 5 min (B), 1 h (C), 2 h (D), 3 h (E), 8 h (F), 32 h (G), 48 h (H) postinjection of P-DOTA-Gd^{3+}. (I–N) Healthy rat images at baseline (I) and 5 min (J), 1 h (K), 2 h (L), 8 h (M), 48 h (N) postinjection of P-DOTA-Gd^{3+}. (O–S) AIA rat images 5 min (O), 2 h (P), 8 h (Q), 32 h (R), and 48 h (S) postinjection of OMNISCAN. (T–X) Healthy rat images at 5 min (T), 1 h (U), 2 h (V), 8 h (W), 48 h (X) postinjection of OMNISCAN.

trast agent, there was substantial MR signal in the kidneys (Fig. 3B). A detailed examination of the single-plane two-dimensional images indicates that at this time most of the contrast is in the kidney cortex with little in the medulla (not shown). Because of the overall increase of the image contrast after the injection, the bladder became evident as a negative image (dark) as is the oval shaped structure at lower left abdominal area. Increased contrast was also observed in the liver, spleen and bone marrow. The major blood vessels were clearly defined while the lesser vessels were not as apparent, probably due to the limited imaging resolution (about 0.5 mm) with the 1.5 T MRI scanner. However, the vessels appear larger, perhaps dilated, than those observed in the healthy controls. Except for some uptake in the bone marrow, little significant contrast signal was evident at this time in the inflamed ankle region.

In the MR images (Fig. 3C) of the AIA rats acquired 1 h postinjection, the signal in the cortex of kidneys was greatly reduced compared with the earlier (5 min) time. However, at this point most of the contrast appeared to be concentrated in the kidney medulla and pelvis. Both ureters contained contrast material and a substantial signal was now evident in the urinary bladder. There appeared to be slight decrease in the MR contrast signal in the liver, spleen and blood vasculature. Interestingly, several "hot spots" started to appear around the tarsus, where the most severe inflammation occurred in this animal model.

From the MR images acquired 2 h (Fig. 3D) and 3 h (Fig. 3E) postinjection of the macromolecular contrast agent, a gradual reduction of MR contrast signal was evident in the kidney (cortex and medulla), liver, spleen, and vasculature. There was, however, an accumulation of the contrast material in the urinary bladder. The "hot spots" detected around tarsus at the 1 h scan continued to expand and increased in contrast in the 2 h (Fig. 4B) and 3 h images.

When the rats were scanned again at 8 h post injection, the MR images (Fig. 3F) showed greatly reduced MR signal in all the vital organs and blood vessels with essentially an undetectable bladder, even though the overall body signal remained slightly greater than that of the baseline images. Surprisingly, however, the MR contrast signal was substantially increased in the ankle joint and metatarsal region (Fig. 4C). The initial "hot spots" disappeared and the MR contrast signal was more evenly distributed around the joint tissue. Also observed was some contrast signal in the posterior knee joints, but with a much lower intensity and size (Fig. 4D).

Subsequently, the animals were again scanned at 32 h and 48 h postinjection, respectively (Figs. 3G and 3H). The overall contrast enhancement of MR signal continued to decline from that observed in the 8 h images. However, the decrease in image contrast in the ankle joint tissue appeared to be much slower than observed in other tissues and organs. Even after 48 h, the enhancing effect of the injected macromolecular contrast agents was still visible in the hind ankle and paw tissue.

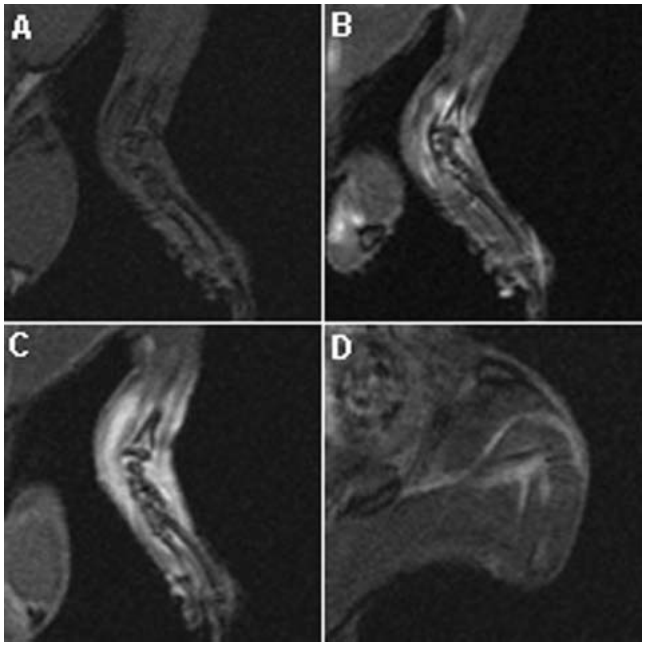

Fig. 4. Single-plane MR images of AIA rats injected with P-DOTA-Gd^{3+}. (A) Baseline MR image of AIA rat. (B) MR image of AIA rat's left ankle and paw, 2 h postinjection. (C) MR image of AIA rat's left ankle and paw, 8 h postinjection. (D) MR image of AIA rat's left knee joint, 8 h postinjection.

Imaging Healthy Rats with P-DOTA-Gd^{3+} as a Contrast Agent

In the MR images (Fig. 3J) taken 5 min after the injection of macromolecular contrast agent, the kidneys of the healthy animals showed extremely strong contrast signal. The single-plane 2D images indicate that the MR contrast resides in both the cortex and medulla (not shown). Both ureters were partially visible. The urinary bladder was filled with a significant amount of contrast medium. Liver, spleen and bone marrow were visible in the image when compared with the baseline image. The major blood vasculatures, including abdominal aorta and inferior vena cava were also highlighted. The arrangement and appearance of these vessels appeared to be normal. No contrast signal was detected outside of the large vessels in the hind paws.

In the MR images taken at 1 h (Fig. 3K) and 2 h (Fig. 3L) postinjection, little contrast media remained in the kidney cortex and medulla, but some contrast signal remained in the kidney pelvis and bladder. The contrast enhancement of the vasculature was slightly reduced compared with that observed at 5 min after injection. At 8 h (Fig. 3M) after injection, the contrast media was completely cleared from the urinary tract. At this time, some of the large vessels were still evident, though less so than at earlier times. The images taken at 48 h (Fig. 3N) after injection replicate the baseline images with no detectable contrast enhancement. As expected, all MR images taken at different times post injection did not show any contrast enhancement in the hind-limb joints of the animal.

Imaging AIA and Healthy Rats with OMNISCAN as a Contrast Agent

The images acquired with the MR enhancement of a low molecular weight paramagnetic contrast agent OMNISCAN (gadolinium complex of diethylenetriamine pentaacetic acid bismethylamide) were obtained similarly as those injected with P-DOTA-Gd^{3+}.

The images (Figs. 3O and 3T) indicated a very fast overall tissue contrast enhancement at 5 min post injection in both healthy and AIA rats. However, the contrast enhancement quickly declined, accompanied by a rapid renal clearance of the contrast medium. At 8 h (Fig. 3Q and 3W), the enhancement was basically gone. Interestingly, the 5 min images (Fig. 3O) of the AIA rats revealed significant contrast enhancement at the inflamed ankle joints, which had cleared at the 2 h scan (Fig. 3P). However, no such observation was found in the healthy rats. Basically, no blood vasculature contrast enhancement could be observed in all OMNISCAN enhanced MR images.

DISCUSSION

Numerous reports have indicated abnormally high plasma protein concentrations in the affected joints of RA patients (4,5,23). Such observations support the concept of using macromolecular delivery systems to specifically target antiarthritic drugs to diseased joints, which may help to achieve superior therapeutic effects. To prove this concept, we used conventional visual examination with Evans blue dye (EB) injection and magnetic resonance imaging (MRI) techniques to follow the *in vivo* fate of macromolecules on an established AIA rat model. Additionally, we histologically confirmed the presence of disease in specific anatomic locations where the MRI technique identified the macromolecular delivery system.

EB is a commonly used agent to assess vascular permeability and integrity (24). It is a dye carrying multiple charges and aromatic structures, which forms a strong complex with plasma albumin. Injection of the dye had been successfully used to establish the concept of macromolecular therapy for the treatment of solid tumors (25). In the present study, we used the EB dye technique in AIA rats to visually assess the accumulation of plasma albumin in inflamed joints. The hind paw of the AIA rats, where the most severe inflammation was evident, readily incorporated the dye compared with that observed in the healthy rats. This observation confirmed that there was indeed a much greater concentration of plasma albumin in the inflamed joints of the AIA rat model.

Though these initial results with EB are significant, interpretation is complicated by the fact that the dye is not covalently bound to albumin and some dye may transfer nonspecifically to other tissues. For example, a slight blue staining was evident in some organs, including the liver and heart.

Therefore, to further support this result, we applied MRI to track the macromolecules injected to AIA rats.

It is well understood that the introduction of paramagnetic contrast agents shortens the longitudinal relaxation time (T_1) of the hydrogen nuclei in tissues (26). The relation between the contrast agent concentration (C) and the T_1 value can be expressed in the following formula, where T_{10} is the initial T_1 relaxation time and r_1 is the relaxivity. Apparently, the increase of contrast agent concentration (C) would lead to the reduction of T_1 value.

$$\frac{1}{T_1} = \frac{1}{T_{10}} + r_1 C \qquad (1)$$

The relation between T_1 and the signal intensity (I) in the MR images is rather complicated. This relation can be expressed as:

$$I = M_0 \frac{(1 - E)\sin(\theta)}{[1 - E\cos(\theta)]} \quad (2)$$

where $E = e^{-T_R/T_1}$, T_R is repetition rate of the imaging sequence and M_0 is the local equilibrium magnetization density. For large tip angles ($\theta = 25°$ or greater) and short T_1, this expression can be approximated as $I = K(1 - E)$ or

$$I = K(1 - e^{-\frac{T_R}{T_1}}) \quad (3)$$

As T_1 gets shorter, the signal intensity (I) increases.

Therefore, correlation of Eqs. 1 and 3 will lead to a qualitative understanding that the higher MR contrast signal intensity in the MR images obtained in this study would represent an existence of higher concentration of the paramagnetic contrast agents in the tissue. Though such relation is not linear and may not be consistent in certain anatomic structures (such as fluid containing GI tract), it is essential for understanding the MR images of the rats in this study.

Conjugation of a low molecular weight paramagnetic contrast agent, DOTA-Gd^{3+} complex to HPMA copolymer permitted the non-invasive monitoring of the fate of the injected polymer in rats with MRI. DOTA-Gd^{3+} is known to be a very stable complex and is considered as inert to *in vivo* dissociation (27,28). *In vitro* transmetallation (major Gd^{3+} dissociation mechanism) study with high concentration of Zn^{2+} for 3 days resulted in retention of more than 98% of the paramagnetic relaxation rate (29). Therefore the enhancement of signal observed in the images is indeed due to the presence of P-DOTA-Gd^{3+} complex in the tissue, not the free Gd^{3+} released from the complex. This approach of labeling the polymer with an MRI contrast agent is similar to other types of studies where the polymers were labeled with fluorochromes to permit localization in organs, tissues and cells (22).

The most significant advantage of MRI, when compared to the radioactive labeling technique and the whole-body scintigraphy (30), is that it illustrates high-resolution three-dimensional anatomic structures of the observed tissue. Such a detailed map of the delivery system deposition within the tissue, when correlated with the local pathologic features, may help to optimize the structure of the drug carrier. Components of the delivery system, including targeting moiety, drug releasing mechanism, and so forth, may be adjusted to achieve superior therapeutic effect. Contrary to the traditional radioactive labeling technique, MRI could not offer quantitative biodistribution data unless a proper *in vivo* calibration is provided.

As shown in Fig. 3, all vital organs in AIA rats showed greater uptake of P-DOTA-Gd^{3+} than the healthy rats. In addition, the clearance of the contrast agent in these organs was slower than those in healthy rats, especially in the kidneys. These observations are consistent with the histologic findings that all organs in AIA rats, including heart, liver, lung, kidney and spleen had some granulomatous chronic inflammation. The vasculature in such inflamed tissues is often more porous, permitting a greater extravasation of macromolecules to the interstitial tissue. This may lead to organ dysfunction, such as the delayed renal clearance of the polymer contrast agent compared to healthy rats. However, the major clearance of P-DOTA-Gd^{3+} from these organs was completed within a few hours (<8 h) in the AIA rats. When compared with normal rats, the major blood vessels appeared to be dilated in the AIA rats. This observation may be due to the up-regulated prostaglandin levels in this systematic inflammation model (31). It may also help to explain the observed faster polymer extravasation.

Interestingly however, extravasation in the inflamed ankle joints was delayed for a short time (1~2 h) in the AIA model (Figs. 3A–3H). The "hot spots" of high MR contrast signal appeared later around the tarsus indicating high local concentrations of P-DOTA-Gd^{3+}. These "hot spots" also reveal the locations of possible local damage in and around the joint. The polymer continues to extravasate, diffuse, accumulate in the ankle joints and the greatest concentrations were observed in the 8 h post injection images (single plane, enlarged MR images, Fig. 4). Because some increased concentrations of polymer were still observed in the joint at 32 h after injection, it appears that the clearance of the polymer from the joint is relatively slow. By correlating the polymer accumulation, as detected by MRI, with the histology of the same tissues (Figs. 2A, 2B, and 2D), it is evident that the accumulation of the polymer correlates with the degree of inflammation. As we observed in the 8 h MR images, the accumulation of P-DOTA-Gd^{3+} to the knee joints was much less than that observed to the ankle joints (Fig. 4D). This finding agrees very well with the amounts and degree of severity of inflammation observed histologically in the joints (Fig. 2F). In contrast to our observation with AIA rats, no extravasation of P-DOTA-Gd^{3+} to the ankle or knee joints was observed in the healthy control rats.

These observations seems to suggest a pharmacokinetic profile with renal clearance mechanism and a redistribution of the HPMA copolymer (labeled with contrast agent) from major organs and blood circulation compartment into the inflammatory arthritic joints. Comparing to the normal animal, the results we obtained from the MR images of the AIA model demonstrate a selective polymer targeting and accumulation effect to the arthritic joints with a time frame of about 1 to 2 days after a single bolus injection. Given that most current anti-arthritic drugs do not specifically target the arthritic joints and damaged tissues coupled with a narrow window of efficacy, the targeting and accumulation of a polymer to an arthritic joint would firmly support the application of macromolecular therapy for the effective delivery and treatment of rheumatoid arthritis. Based on the same principle, promising results have been obtained using stealth liposomes containing glucocorticoid in the treatment of collagen-induced arthritis in mice (13,32). But the well-documented accumulation of the liposomes in liver and spleen is undesirable (33). Water-soluble polymeric drug carriers, such as HPMA copolymers are known to possess biodistribution profiles with reduced accumulation in the liver and the spleen (34). In addition, proper design of linkage between the drug and the polymer backbone would allow the drug release to be triggered by local pathologic factors, such as low pH, elevated enzyme activity, hypoxia, etc. Therefore, a well-controlled local drug release profile may be achieved (11).

While the enhanced permeability of the vasculature in the arthritic joints may be comparable to those found in solid tumors, it is possible that the retention of the polymer in the joint tissue is weaker, as evidenced by the shorter accumulation time. It may be attributed to elevated intraarticular pressure (35) and the existence of lymphatic vessels, though they might have been partially damaged or deformed (6,7). Therefore, the design of the polymeric antiarthritic drug delivery systems must be different from those used in the treatment of solid tumors.

Due to the nature of the short polymer accumulation time frame we observed, it is apparent that a swift drug-cleavage mechanism should be applied to ensure effective releasing of drug from the proposed macromolecular carrier. There are some pathologic features of the arthritic joints that may be exploited for this. The release of the drug from the polymer may be facilitated by things such as the very high extracellular enzyme activities (e.g. cathepsin K and MMPs) (36), low pH, hypoxia or elevated temperature (37). Likewise, measures that would enhance the retention of the extravasated polymers in the joints may also be considered in the design of the polymer drug conjugates. Incorporation of targeting moieties, which would bind to the negatively charged cartilage (38), the freshly eroded bone surface (22) or the enriched rheumatic factors in the RA joints may also increase the uptake and retention of the polymer in joint tissue. It is also possible that by increasing the molecular weight of the polymeric carrier, a greater retention of the polymer in the RA joint may occur. Antiarthritic drugs with fast therapeutic effects, such as glucocorticoids may be considered as one of the efficient candidates for such delivery systems.

The results obtained in this study may also be beneficial for the improvement of currently available protein drugs and orally available low molecular weight drugs. As we observed in this study, the extravasation of the injected polymer into the RA joints was delayed for 1 to 2 h. Thus, for the protein or peptide drugs, they must survive this period of time against hepatic and renal clearance. Seemingly, modifications of the proteins with semitelechelic polymer, such as polyethylene glycols (PEGs) may represent a good approach in solving this problem (3). Currently, screening of low molecular weight drug candidates seems to be largely dependent on their therapeutic potency demonstrated in *in vitro* assays. However, current studies suggest that the albumin binding capacity should be another important factor to consider in drug candidate selection. A molecule, which has strong albumin binding ability, could lead to longer half-life and higher local bioavailability in the RA joints. In this case, the plasma albumin may be considered as its natural macromolecular carrier, which could take the advantage of the joint-selective accumulation effect we observed in the study.

Clearly, the macromolecular MRI contrast agent we used in this study permits a much longer imaging time frame compared to low molecular weight contrast agents, such as OMNISCAN (Fig. 3). This long retention and local accumulation of the contrast agent would allow more sophisticated imaging procedures to be performed, which may lead to better quality images of the arthritic joints. Per conjugation with molecular imaging agents, the macromolecular delivery system would also help to noninvasively probe the pathogenesis of rheumatoid arthritis.

CONCLUSIONS

Using modern MR imaging techniques, we observed the selective accumulation of macromolecules in arthritic joints of AIA rats. There was an excellent correlation between the uptake and retention of the MR contrast agent labeled polymer with histopathological features of inflammation and local tissue damage. These findings also correlated well with the observations of the Evans blue injected AIA rats. Based on these results, we suggest that specially designed macromolecular delivery systems would be beneficial in the improvement of current imaging and treatments for rheumatoid arthritis.

ACKNOWLEDGMENTS

This work was supported in part by NIH grant EB00251 (DW, MS, PK and JK) and AR44806 (SCM). We acknowledge Dr. Rock Hadley for the coil that we used in this study. We also thank Dr. L. D. McGill of ARUP Veterinary Service at University of Utah for his help with part of the pathological analysis.

REFERENCES

1. G. S. Firestein. Etiology and Pathogenesis of Rheumatoid Arthritis. In S. Ruddy, E. D. Harris Jr. and C. B. Sledge (eds.), *Kelley's Textbook of Rheumatology,* 6th Ed. W.B. Saunders, St. Louis, 1997, pp. 921.
2. F. C. McDuffie. Morbidity impact of rheumatoid arthritis in society. *Am. J. Med.* **78**:1–5 (1985).
3. J. S. Smolen and G. Steiner. Therapeutic strategies for rheumatoid arthritis. *Nat. Rev. Drug Discov.* **2**:473–488 (2003).
4. W. J. Wallis, P. A. Simkin, and W. B. Nelp. Protein traffic in human synovial effusion. *Arthritis Rheum.* **30**:57–63 (1987).
5. J. R. Levick. Permeability of rheumatoid and normal human synovium to specific plasma proteins. *Arthritis Rheum.* **24**:1550–1560 (1981).
6. M. Albuquerque and J. P. de Lima. Articular lymphoscintigraphy in human knees using radiolabeled dextran. *Lymphology* **23**:215–218 (1990).
7. L. S. Wilkinson and J. C. W. Edwards. Demonstration of lymphatics in human synovial tissue. *Rheumatol. Int.* **11**:151–155 (1991).
8. E. L. Matteson. Current treatment strategies for rheumatoid arthritis. *Mayo Clin. Proc.* **75**:69–74 (2000).
9. E. Santana-Sahagun and M. H. Weisman. Nonsteroidal Antiinflammatory Drugs. In S. Ruddy, E. D. Harris Jr. and C. B. Sledge (eds.), *Kelley's Textbook of Rheumatology,* 6th Ed. W.B. Saunders, St. Louis, 1997, pp. 799–822.
10. C. M. Stein and T. Pincus. Glucocorticoids. In S. Ruddy, E. D. Harris Jr. and C. B. Sledge (eds.), *Kelley's Textbook of Rheumatology,* 6th Ed. W.B. Saunders, St. Louis, 1997, pp. 823–840.
11. J. Kopeček, P. Kopečková, T. Minko, and Z. R. Lu. HPMA copolymer-anticancer drug conjugates: design, activity, and mechanism of action. *Eur. J. Pharm. Biopharm.* **50**:61–81 (2000).
12. L. W. Seymour. Passive tumor targeting of soluble macromoleculaes and drug conjugates. *Crit. Rev. Ther. Drug Carrier Syst.* **9**: 135–187 (1992).
13. J. M. Metselaar, M. H. Wauben, J. P. Wagenaar-Hilbers, O. C. Boerman, and G. Storm. Complete remission of experimental arthritis by joint targeting of glucocorticoids with long-circulating liposomes. *Arthritis Rheum.* **48**:2059–2066 (2003).
14. M. N. J. Paley, I. D. Wilkinson, E. van Beek, and P. D. Griffiths. Magnetic resonance imaging: basic principles. In R. G. Grainger, D. Allison, A. Adam and A. K. Dixon (eds.) *Grainger & Allison's Diagnostic Radiology: A Textbook of Medical Imaging,* 4th Ed. Churchill Livingstone, Inc., London, 2001, pp. 101–136.
15. J. Kopeček and H. Bažilová. Poly[N-(2-hydroxypropyl)methacrylamide]. I. Radical polymerization and copolymerization. *Eur. Polym. J.* **9**:7–14 (1973).
16. V. Omelyanenko, P. Kopečková, and C. Gentry. and J. Kopeček. Targetable HPMA copolymer-adriamycin conjugates. Recogni-

tion, internalization, and subcellular fate. *J. Control. Rel.* **53**:25–37 (1998).
17. T. H. Cronin, H. Faubl, W. W. Hoffman, and J. J. Korst. Xylenediamines as antiviral agents. U.S. Patent 4,034,040 (1977).
18. S. Moore and W. H. Stein. A modified ninhydrin reagent for the photometric determination of amino acids and related compounds. *J. Biol. Chem.* **211**:907–913 (1954).
19. L. W. Seymour, R. Duncan, J. Strohalm, and J. Kopecek. Effect of molecular weight (Mw) of N-(2-hydroxypropyl)methacrylamide copolymers on body distribution and rate of excretion after subcutaneous, intraperitoneal, and intravenous administration to rats. *J. Biomed. Mater. Res.* **21**:1341–1358 (1987).
20. Z. R. Lu, X. Wang, D. L. Parker, K. C. Goodrich, and H. R. Buswell. Poly(L-glutamic acid) Gd(III)-DOTA conjugate with a degradable spacer for magnetic resonance imaging. *Bioconjug. Chem.* **14**:715–719 (2003).
21. A. M. Bendele. Animal models of rheumatoid arthritis. *J. Musculoskel. Neuron. Interact.* **1**:377–385 (2001).
22. D. Wang, S. C. Miller, M. Sima, and P. Kopečková, and J. Kopeček. Synthesis and evaluation of water-soluble polymeric bone-targeted drug delivery systems. *Bioconjug. Chem.* **14**:853–859 (2003).
23. I. Kushner and J. A. Somerville. Permeability of human synovial membrane to plasma proteins. Relationship to molecular size and inflammation. *Arthritis Rheum.* **14**:560–570 (1971).
24. T. P. Jacobs, O. Kempski, D. McKinley, A. J. Dutka, J. M. Hallenbeck, and G. Feuerstein. Blood flow and vascular permeability during motor dysfunction in a rabbit model of spinal cord ischemia. *Stroke* **23**:367–373 (1992).
25. Y. Matsumura and H. Maeda. A new concept for macromolecular therapeutics in cancer chemotherapy: mechanism of tumoritropic accumulation of proteins and the antitumor agent smancs. *Cancer Res.* **46**:6387–6392 (1986).
26. G. Marchal, H. Bosmans, and S. J. McLachlan. Magnetopharmaceuticals as Contrast Agents. In E. J. Potchen, E. M. Haacke, J. E. Siebert, A. Gottschalk (eds.), *Magnetic Resonance Angiography, Concepts and Applications.* Mosby Publishing, St. Louis, 1993, pp 305–322.
27. P. Wedeking, K. Kumar, and M. F. Tweedle. Dissociation of gadolinium chelates in mice: relationship to chemical characteristics. *Magn. Reson. Imaging* **10**:641–648 (1992).
28. J. S. Mann. Stability of gadolinium complexes in vitro and in vivo. *J. Comput. Assist. Tomogr.* **17**:S19–S23 (1993).
29. S. Laurent, L. V. Elst, F. Copoix, and R. N. Muller. Stability of MRI paramagnetic contrast media: a proton relaxometric protocol for transmetallation assessment. *Invest. Radiol.* **36**:115–122 (2001).
30. E. T. Dams, W. J. Oyen, O. C. Boerman, G. Storm, P. Laverman, P. J. Kok, W. C. Buijs, H. Bakker, J. W. van der Meer, and F. H. Corstens. ^{99m}Tc-PEG liposomes for the scintigraphic detection of infection and inflammation: clinical evaluation. *J. Nucl. Med.* **41**: 622–630 (2000).
31. D. Claveau, M. Sirinyan, J. Guay, R. Gordon, and C. C. Chan. Y. Bureau, D. Riendeau and J. A. Mancini. Microsomal prostaglandin E synthase-1 is a major terminal synthase that is selectively up-regulated during cyclooxygenase-2-dependent prostaglandin E_2 production in the rat adjuvant-induced arthritis model. *J. Immunol.* **170**:4738–4744 (2003).
32. J. M. Metselaar, W. B. van den Berg, A. E. Holthuysen, M. H. Wauben, G. Storm, and P. L. van Lent. Liposomal targeting of glucocorticoids to synovial lining cells strongly increases therapeutic benefit in collagen type II arthritis. *Ann. Rheum. Dis.* **63**:348–353 (2004).
33. A. Gabizon, D. Goren, A. T. Horowitz, D. Tzemach, A. Lossos, and T. Siegal. Long-circulating liposomes for drug delivery in cancer therapy: a review of biodistribution studies in tumor-bearing animals. *Adv. Drug Deliv. Rev.* **24**:337–344 (1997).
34. R. Duncan. The dawning era of polymer therapeutics. *Nat. Rev. Drug Discov.* **2**:347–360 (2003).
35. M. I. V. Jayson and A. St. J. Dixon. Intra-articular pressure in the rheumatoid arthritis of knee. I. Pressure changes during passive joint distension. *Ann. Rheum. Dis.* **29**:261–265 (1970).
36. Y. Okada. Proteinases and Matrix Degradation. In S. Ruddy, E. D. Harris Jr. and C. B. Sledge (eds.), *Kelley's Textbook of Rheumatology,* 6th Ed. W.B. Saunders, St. Louis, 1997, pp. 55–72.
37. P. S. Treuhaft and D. J. McCarty. Synovial fluid pH, lactate, oxygen and carbon dioxide partial pressure in various joint diseases. *Arthritis Rheum.* **14**:475–484 (1971).
38. I. Giraud, M. Rapp, J. C. Maurizis, and J. C. Madelmont. Application to a cartilage targeting strategy: synthesis and in vivo biodistribution of ^{14}C-labeled quaternary ammonium-glucosamine conjugates. *Bioconjug. Chem.* **11**:212–218 (2000).